

# Preparation and characterization of a bi-layered nano-filtration membrane from a chitosan hydrogel and bacterial cellulose nanofiber for dye removal

Cai Zhijiang  · Xiong Ping · Zhu Cong · Zhai Tingting · Guo Jie · Zhao Kongyin

Received: 1 December 2017 / Accepted: 27 June 2018 / Published online: 30 June 2018  
© Springer Nature B.V. 2018

**Abstract** A novel nanofiber composite nano-filtration membrane was prepared by combination of grafting, electrospinning and surface coating. First, carboxyl multi-walled carbon nanotubes were grafted onto bacterial cellulose molecular chains by solution reaction. The grafting products were characterized by TEM, FTIR, Raman, XPS and TGA measurements. Then, they were electrospun into nanofibers to be the supporting layer, and a coating of denser chitosan hydrogel thin film was used as the barrier layer. The morphology of the electrospun nanofibers and composite membrane were observed by SEM. The mechanical behavior of the composite membrane was investigated in dry and wet state. The filtration properties were evaluated in term of the pure water flux (PWF), dye rejection rate and anti-fouling properties. Results showed that the chitosan hydrogel coated electrospun nanofiber composite membrane had higher tensile strength and Young's Modulus with the value of 11.75, 10.11 and 244, 211 MPa in dry and wet state, respectively. The PWF was increased from 52.1 to 140.7 L/m<sup>2</sup> h with the operation pressure increasing from 0.1 to 0.6 MPa. Direct Orange S, Procion Red mx-5B, Stilbene Yellow and Methylene

Blue with molecular weight ranged from 300 to 800 g/mol were selected for dye removal test. The rejection rate could maintain over 90% for dyes with the molecular weight larger than 600 g/mol under 0.5 MPa. The chitosan hydrogel coated electrospun nanofiber composite membrane exhibited good anti-fouling properties for both oil and protein. These results indicate that these membranes are efficient for dye removal from wastewater, with high flux and rejection rate at high pressure.

**Keywords** Carbon nanotubes · Electrospinning · Chitosan · Nano-filtration · Dye rejection

## Introduction

Membrane separation technology possesses the advantages of low energy consumption, high efficiency and simple device operation. Nano-filtration membranes are used extensively for wastewater treatment, especially for removal of dyes and other small molecules, heavy metal ions, and nano-particles (Xu et al. 2012; Zhu et al. 2015; Zeng et al. 2016; Rajesh et al. 2013; Urban 2016).

Membranes for removal of dyes from wastewater require nano-filtration technology due to the average molecular weights of the majority dyes being in the range of 100–1000 Da for which nano-filtration membranes have a high rejection rate (Zheng et al.

C. Zhijiang (✉) · X. Ping · Z. Cong · Z. Tingting · G. Jie · Z. Kongyin  
State Key Laboratory of Separation Membranes and Membrane Processes, School of Textiles, Tianjin Polytechnic University, Tianjin, China  
e-mail: caizhijiang@hotmail.com

2013; Zhang et al. 2015; Li et al. 2014). However, nano-filtration membranes usually have low porosity and pores that are less connected, so that the flux is low at low pressure and the pores block easily (Zhao and Wang 2017; Kebria et al. 2015; Liang et al. 2014; Gasemloo et al. 2016). Many efforts have been made to improve the flux of the nano-filtration membranes by changing the structures and properties of the supporting layer and the barrier layer (Wu et al. 2014; Zhu et al. 2011; Zhou et al. 2014; Kaur et al. 2012a, b; Lalia et al. 2013). Use of a nanofiber membrane as the supporting layer should be a good candidate to improve dye removal membrane.

Electrospinning is an effective technique that has been widely used for the fabrication of continuous nanofiber membrane with high porosity above 80% and interconnected pore structure (Liu et al. 2016; Huang et al. 2017; Ahmed et al. 2015). The electrospun nanofiber membrane can be applied in tissue engineering (Khorshidi et al. 2016), wound dressings (Rosa et al. 2017), bio-sensors (Zhang et al. 2017), energy storage device (Cai and Zhang et al. 2017), air filtration (Zhu et al. 2017), metal ions adsorption (Cai et al. 2017a, b) and membrane filtration technology (Makaremi et al. 2016). Kaur et al. (2012a, b) prepared a highly hydrophilic electrospun membrane based on PVDF material by blending this polymer with surface modifying macromolecules prepared from urethane pre-polymer with poly(propylene glycol) and poly(ethylene glycol) with average molecular weights of 1000 Da. The pure water flux was 20% higher than that of non-blended electrospun PVDF membrane. However, electrospinning technology is difficult to produce dense membranes that are required for nano-filtration membrane separation, and the nanofibrous membranes possess poor flux stability and anti-fouling property for small molecular solution, but they may provide a better supporting layer for currently used phase inversion nano-filtration membranes (Wang et al. 2010; Guo et al. 2016). Yoon et al. (2009) prepared high flux nano-filtration membranes based on interfacially polymerized polyamide barrier layer on electrospun polyacrylonitrile nanofibrous scaffolds. And the permeate flux was about 38% higher than commercial NF270 membrane with the similar rejection rate for divalent salt solution. However, little literature about hydrogel coated electrospun membrane as nano-filtration membrane for dye removal has been reported.

In this paper, chitosan hydrogel coated electrospun bacterial cellulose composite nanofiber nano-filtration membrane was prepared by electrospinning and surface coating method. To improve the tensile performances of electrospun nanofiber supporting layer, carbon nanotubes were grafted onto bacterial cellulose molecular chains. Adhesion between chitosan hydrogel top barrier layer and electrospun bacterial cellulose supporting layer was enhanced by cross-linking. The morphology, tensile mechanical performances, oil–water separation and dye rejection properties of the hydrogel coated nanofiber composite membrane were systematically investigated.

## Experimental

### Materials

Bacterial cellulose (BC,  $M_w = 6.3 \times 10^5$  g/mol) and chitosan ( $M_w = 10^5$  g/mol, 83% degree of deacetylation) were provided by Tianjin GreenBio Materials Co., Ltd. Carboxyl multi-walled carbon nanotubes (cMWCNTs) were purchased from Nanjing XFNANO Materials Tech Co., Ltd. N,N-Dimethylacetamide (DMAc), LiCl, ethanol, acetic acid, glutaraldehyde, Tween-80, 0# diesel, MgSO<sub>4</sub> and NaCl were purchased from Tianjin Kemiou Chemical Reagent Co., Ltd. Bovine serum albumin (BSA,  $M_w = 67$  kDa) was obtained from Sigma. Direct Orange S ( $M_w = 756.67$  g/mol), Procion Red mx-5B ( $M_w = 615.33$  g/mol), Stilbene Yellow ( $M_w = 452.37$  g/mol) and Methylene Blue ( $M_w = 337.87$  g/mol) were purchased from Tianjin Umbrella Science & Technology Co. Ltd.

### Preparation of cMWCNTs grafted BC

The preparation of carboxyl multi-walled carbon nanotubes grafted BC (BC-g-cMWCNTs) was carried out by the following procedures. First, 9.05 g of LiCl and 100 mL of DMAc were measured into a three-neck flask. The mixture was heated at 130 °C until the LiCl dissolved completely. Then, 0.05 g of cMWCNT were added with continuous stirring and ultrasonic dispersing for 180 min. After that, 0.5 g of BC powder were dissolved in the dispersion and stirred for 6 h, which was kept at 20 °C under nitrogen. Simultaneously, the flask was placed in a thermostatic bath at 70 °C, and the catalyst, 0.02 g of stannous octoate

were then dropped slowly and stirred for reaction for 12 h. The adequate amount of ethanol was added into the reaction product with stirring, which at this stage was in the form of a suspension, and then filtered under room condition and dried overnight under vacuum. The reaction products was dissolved in excess DMAc/LiCl co-solvent system again and filtered to remove un-reacted BC homopolymer and stannous octoate through the PTFE membrane. The dissolution and filtration processes were repeated several times. BC-g-cMWCNTs was finally obtained after drying overnight under vacuum.

#### Preparation of electrospun BC-g-cMWCNTs nanofibers

5 wt% BC-g-cMWCNTs spinning solution was prepared by dissolving BC-g-cMWCNTs powder in DMAc/LiCl co-solvent system with continuously stir. The electrospun BC-g-cMWCNTs nanofibers were produced by the following electrospinning parameters: an applied voltage of 22 kV, a polymer-flow-rate of 1.5 mL/h, a collecting distance of 20 cm, and spinneret inner diameter of 0.6 mm. All experiments were done in an environmental chamber with constant temperature at 25 °C and relative humidity of 35%.

#### Preparation of chitosan coated electrospun BC-g-cMWCNTs nanofiber composite membrane

The preparation of chitosan coated electrospun BC-g-cMWCNTs nanofiber composite membrane was schematically shown in Fig. 1. The homogeneous coating solution with 2.0 wt% chitosan was prepared by dissolving chitosan powder in acetic acid. Then the dilute solution was outspread on electrospun BC-g-cMWCNTs nanofibers by a glass rod enlaced with brass wire. The chitosan coated electrospun BC-g-cMWCNTs nanofiber membrane was immediately immersed in 2.0 wt% glutaraldehyde aqueous solution for cross-linking for 12 h. Thus, the chitosan coated electrospun BC-g-cMWCNTs nanofiber composite membrane was obtained.

#### Characterization

Transmission electron microscopy (TEM, JEM-1200EX, Japan) was used to investigate the morphology of BC-g-cMWCNTs at an accelerating voltage of

100 kV. The Fourier Transform Infrared spectroscopy (FTIR, TENSOR37, Bruker, German) and Raman spectrophotometer (Jobin-Yvon T64000) were used to analyze the changes of the internal molecular structure of BC-g-cMWCNTs. The X-ray photoelectron spectroscopy (XPS, K-alpha, ThermoFisher, England) was used to analyze the chemical composition of BC-g-cMWCNTs surface. The TGA analysis for BC-g-cMWCNTs (TGA, STA409PC, NETZSCH, German) was performed under nitrogen heating from room temperature to 800 °C at rate of 5 °C/min. Scanning electron microscope (SEM, HITACHI, Japan) was used to observe the morphology of electrospun BC-g-cMWCNTs nanofibers and chitosan coated electrospun BC-g-cMWCNTs nanofiber membrane. To calculate average diameter of electrospun nanofibers, one hundred electrospun fibers were randomly selected from five SEM images and measured by Image-Pro Plus software. The tensile mechanical properties of nanofiber membranes were determined by the universal testing machine (LLY-06F, China). The nanofiber membranes were first cut into rectangle samples with 10 mm long and 5 mm wide. Then, the samples were fixed at machine and stretched at a constant speed of 10 mm/min. The thickness of the samples was measured by a digital micrometer gauge. For each test, ten samples were used to calculate average value and deviation.

#### Filtration properties evaluation

The filtration performances of chitosan coated electrospun BC-g-cMWCNTs nanofiber composite membrane were evaluated by measuring the flux and rejection rate for dye solution using a membrane filtration device assembled by our lab as shown in Fig. 2. The membrane filtration device was equipped with pressure-control unit with filtration area of 70.65 cm<sup>2</sup>. The diameter and thickness of the circular membrane used in the test are 40 mm and about 35 μm, respectively. First, 0.1 g/L emulsified oil-water solution, 0.1 g/L BSA aqueous solution, 0.1 g/L Direct Orange S, 0.1 g/L Procion Red mx-5B aqueous solutions, 0.1 g/L Stilbene Yellow aqueous solutions, 0.1 g/L Methylene Blue aqueous solutions, 2000 mg/L MgSO<sub>4</sub> and 2000 mg/L NaCl were prepared and used as feed solution. The filtration process was carried out under room condition at an applied pressure in the range of 0.1–0.6 MPa for 180 min.

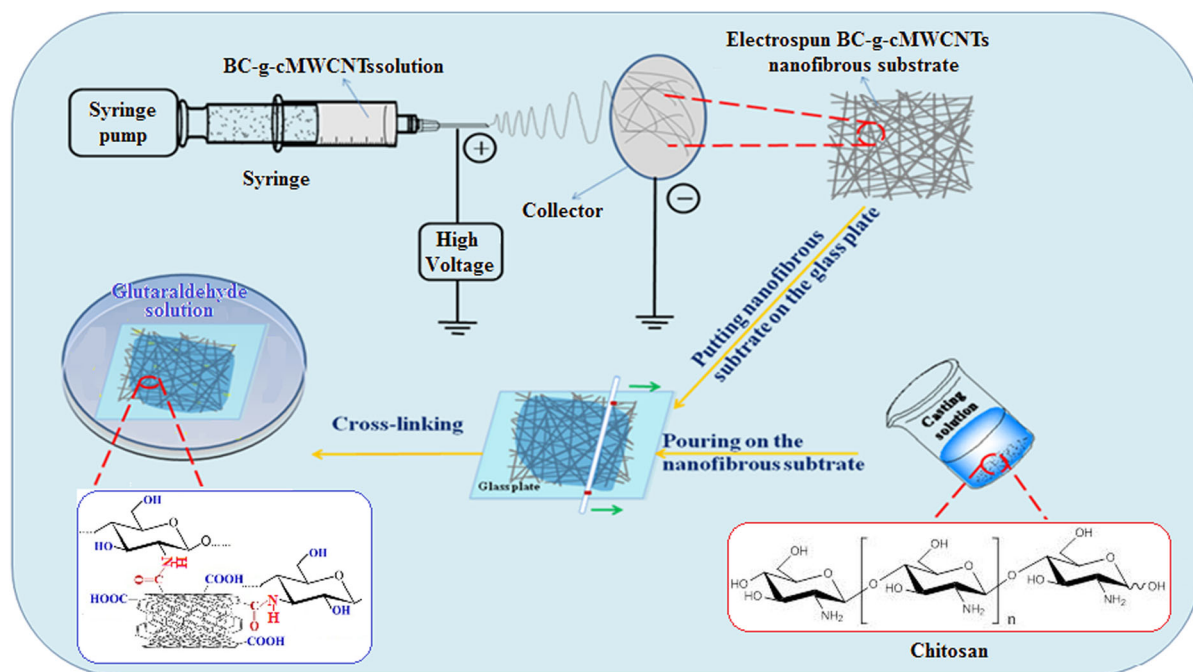


**Fig. 1** The preparation process for chitosan coated electrospun BC-g-cMWCNTs nanofiber composite membrane

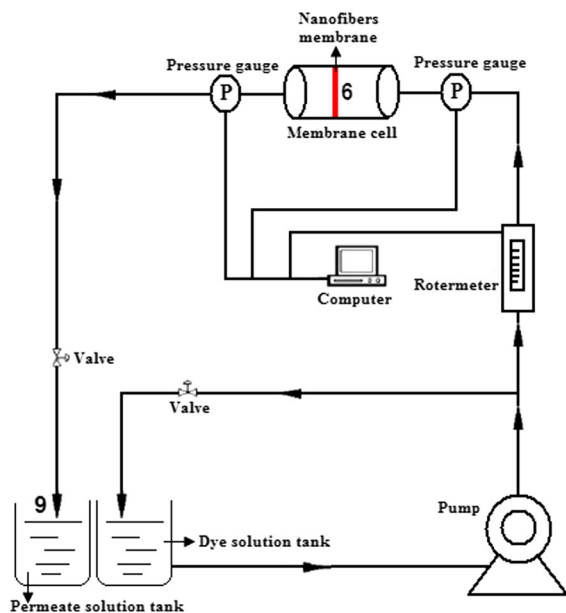


**Fig. 2** The diagram of the membrane filtration device

The solution concentration ( $C_p$ , mg/L) and volume ( $V$ , L) permeated the filtration membrane were measured by UV spectrophotometer and recorded as a function of time. The rejection rate ( $R$ , %) and solution flux ( $J$ , L/m<sup>2</sup> h) were determined using the Eqs. (1) and (2).

$$R = \left(1 - \frac{C_p}{C_0}\right) \times 100\% \quad (1)$$

$$J = \frac{V}{A \times t} \quad (2)$$

where  $C_p$  and  $C_0$  are the concentrations of the permeate and feed, respectively.  $A$  is the filtration area of membrane (m<sup>2</sup>) and  $t$  is the filtration time (h).

## Results and discussion

### Preparation and Characterization of BC-g-cMWCNTs

#### Preparation of BC-g-cMWCNTs

Carbon nanotubes have excellent mechanical and electrical properties as a reinforcing material. Functionalized carbon nanotubes have been widely used for preparation of polymer-g-CNT materials due to surface functional groups, which can react with other functional groups of polymer matrix (Wenhui et al. 2007). PLA-g-CNT (Yoon et al. 2010), Chitosan-g-CNT (Yang et al. 2015) and PHB-g-CNT (Cai et al.

2018) materials have been reported by condensation reaction between the functional groups like hydroxyl groups, amine groups and carboxylic groups. In this paper, cMWCNTs have been grafted onto BC molecular chains by condensation reaction between the carboxylic groups of cMWCNTs and hydroxyl groups of BC as depicted in Fig. 3. The presence of covalently bond between BC and cMWCNTs was investigated by taking FT-IR, Raman and XPS spectra. The quantity of cMWCNTs grafted on BC was estimated by TGA measurement. It was expected that the introduction of cMWCNTs may enhance the mechanical properties of the electrospun BC nanofiber membrane.

### FTIR and Raman spectra

Figure 4a depicts the FTIR spectra of BC and BC-g-cMWCNTs samples. In the case of pure BC, the broad band at  $3450\text{ cm}^{-1}$  was attributed to O–H stretching vibration. Band at  $2820\text{ cm}^{-1}$  represented the aliphatic C–H stretching vibration. The sharp and steep band observed at  $1080\text{ cm}^{-1}$  was due to the presence of C–O–C stretching vibrations. In the spectrum of BC-g-cMWCNTs, the band of stretching vibration of -OH was shifted to lower wavenumbers ( $3424\text{ cm}^{-1}$ ) and the intensity was obviously weakened. A new absorption band located at  $1735\text{ cm}^{-1}$  can be detected, which was assigned to the characteristic peak of C=O bond. It

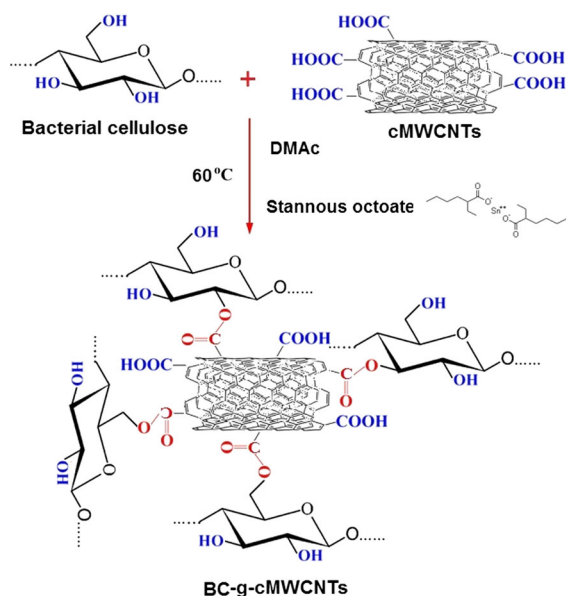


**Fig. 3** Schematic illustration of the grafting process

clearly indicates the formation of new ester bond between the BC and cMWCNTs as the results of the molecular interaction presented between the -OH of BC and -COOH of cMWCNTs.

Figure 4b shows the Raman spectra of cMWCNTs and BC-g-cMWCNTs. For pristine cMWCNTs, two peaks located at  $1365$  and  $1595\text{ cm}^{-1}$  can be observed, which were ascribed to the D-mode and G-mode of cMWCNTs corresponding to disorder induced mode and tangential mode, respectively (Jorio et al. 2003). In the case of BC-g-cMWCNTs, a new shoulder peak located at  $1615\text{ cm}^{-1}$  can be detected, which was associated with defects and disorder induced features in cMWCNTs. This result indicates that a new covalent bond formation in the BC-g-cMWCNTs.

### XPS analysis

Figure 5 presents the XPS spectra of BC, cMWCNTs and BC-g-cMWCNTs. For BC, two peaks at binding energies of 284.46 and 542.14 eV were assigned to C(1s) and O(1s) orbit. The mass percentage of main elements of C and O was 64.8 and 35.2%. For cMWCNTs, the amount ratio of C:O was 95.4:4.6, which included the C in C–C bond and the C in C–O bond existed in functional groups. For BC-g-cMWCNTs, the amount ratio of C:N was 72.6:27.4. The amount of carbon was higher than that of BC. None of Sn element could be detected by XPS in BC-g-cMWCNTs, which indicated that the stannous octoate was completely removed by post-treatment. The element of C existed in the BC-g-cMWCNTs was mainly attributed to the hydrocarbon bond (C–H) or the carbon–carbon bond (C–C), the carbon–oxygen bond (C–O) and ester groups (O–C=O) in carbonyl and alcoholic hydroxyl groups, corresponding to binding energy of 284.32, 285.67, 286.83 and 289.31 eV, respectively. The presence of a large number of carbonyl and alcoholic hydroxyl groups indicated that cMWCNTs were introduced onto BC molecular chains. Moreover, the formation of a large number of ester groups confirmed the occurrence of grafting reaction.

### TGA measurement

Thermo-gravimetric analysis (TGA) is a continuous process, involving the measurement of sample weight in accordance with increasing temperature in the form

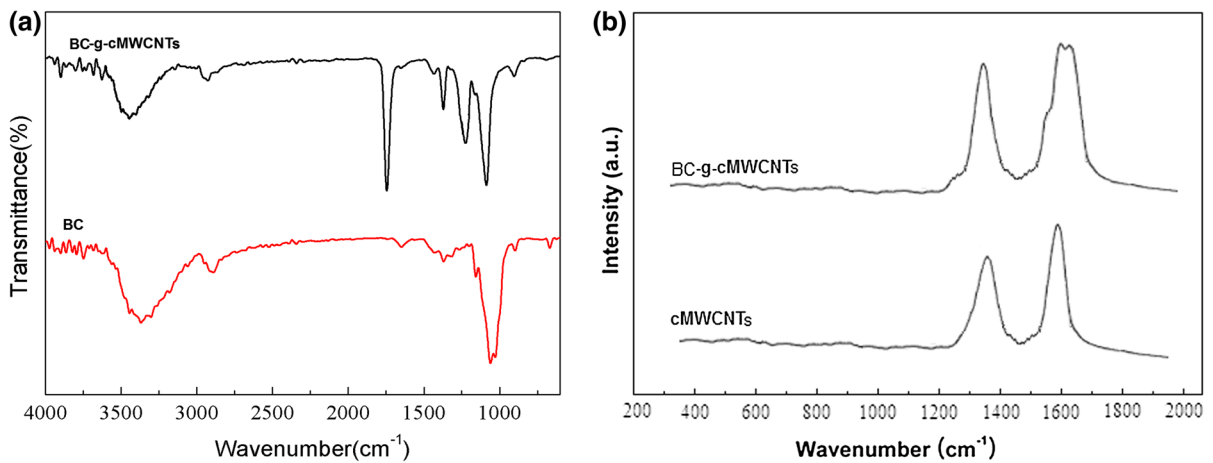


**Fig. 4** FTIR spectra (a) of BC and BC-g-cMWCNTs and Raman spectra (b) of cMWCNTs and BC-g-cMWCNTs

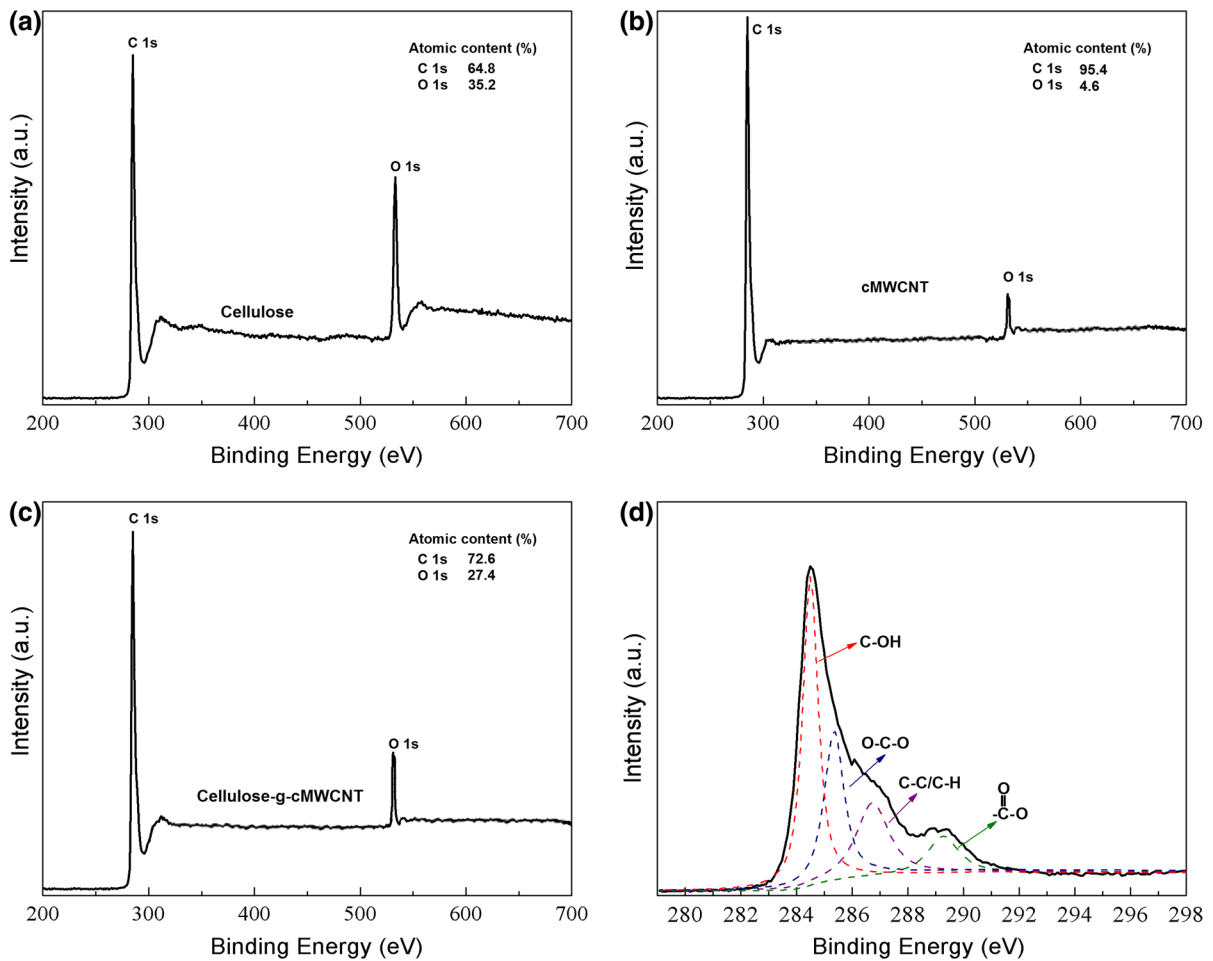


**Fig. 5** The XPS spectra of BC (a), cMWCNTs (b), BC-g-cMWCNTs (c) and C1 s spectrum of BC-g-cMWCNTs (d)

of programmed heating. To estimate quantity of cMWCNTs grafted on BC, TGA measurements for cMWCNTs, BC and BC-g-cMWCNTs were performed and the results are given in Fig. 6. For cMWCNTs, there was almost no weight loss (< 0.5%) below 300 °C. The weight loss of the cMWCNTs mainly happened in the temperature ranged from 300 to 800 °C. The percentage weight loss at 800 °C was about 7.46% for cMWCNTs due to the decomposition of carboxyl groups on the surface of cMWCNTs. In case of BC and BC-g-cMWCNTs, the weight loss curves can be divided into two stages. In stage I, the weight loss was very low (< 3%), which was ascribed to evaporation of physically absorbed water molecules at the temperature below 200 °C. In stage II, the major weight loss corresponding to decomposition of BC molecules was happened at the temperature ranged from 200 to 500 °C. It can be seen that the thermal decomposition temperature of BC-g-cMWCNTs was higher than that of pure BC. The thermal decomposition temperature (50% mass loss) was about 256.8 °C for pure BC and 278.4 °C for BC-g-cMWCNTs. This result indicated that BC-g-cMWCNTs showed improved thermal stability comparing with pure BC. Since the thermal decomposition temperature is affected by the structural parameters such as molecular weight, crystallinity, orientation as well as intermolecular interaction. We believe that this increase in thermal stability for BC-g-cMWCNTs might be due to the grafting reaction by ester bonds formed by –OH groups of BC and –COOH groups of

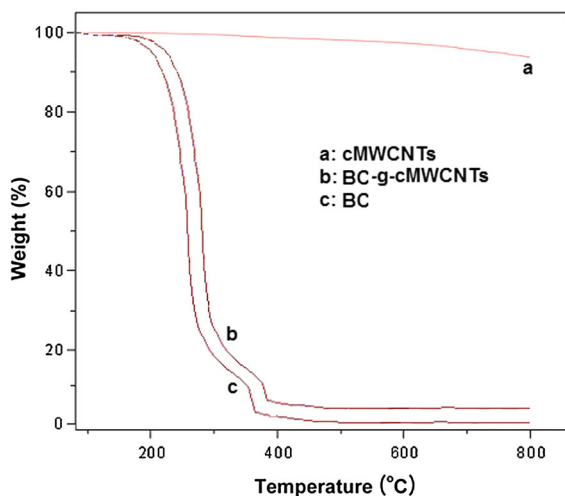


**Fig. 6** TGA curves of cMWCNTs, BC and BC-g-cMWCNTs

cMWCNTs. By comparing the weight loss of the BC-g-cMWCNTs with cMWCNTs and BC, the ratio of cMWCNTs grafted on BC in BC-g-cMWCNT was calculated to be approximately 3.64%.

#### TEM observation

Figure 7 shows the TEM images of BC-g-cMWCNTs. The BC molecules were uniformly coated on the surface wall of cMWCNTs. The outer diameter of cMWCNTs was increased from 10.68 to 17.31 nm due to the grafting of BC molecules. This result indicated that the grafting reaction occurred between BC molecules and cMWCNTs, and the BC molecular chains wrapped around the wall of cMWCNTs.

Morphology and physical properties of chitosan coated BC-g-cMWCNTs nanofiber composite membrane

#### Morphology

Figure 8a and b demonstrate the SEM image and the diameter distribution of electrospun BC-g-cMWCNTs nanofiber. The electrospun BC-g-cMWCNTs nanofiber presented smooth surface morphology, interconnected pore structure and three-dimensional random arrangement. The diameter was distributed in the range of 400–700 nm with average value of 512 nm. Figure 8c and d show the surface and cross section morphology of chitosan coated BC-g-cMWCNTs nanofiber composite membrane. The surface morphology was smooth and uniform, no pores and defects can be observed. Chitosan coating can decrease the roughness of electrospun BC-g-cMWCNTs nanofiber membrane. From cross section morphology, we can see a few microns chitosan hydrogel thin film coated on the surface of electrospun BC-g-cMWCNTs nanofiber membrane. The thickness of chitosan coated BC-g-cMWCNTs nanofiber composite membrane was about 30 μm.

#### The mechanical properties

Figure 9 demonstrates the stress–strain curves of chitosan membrane and chitosan coated BC-g-cMWCNTs nanofiber composite membrane. Both chitosan membrane and chitosan coated BC-g-cMWCNTs nanofiber composite membrane showed

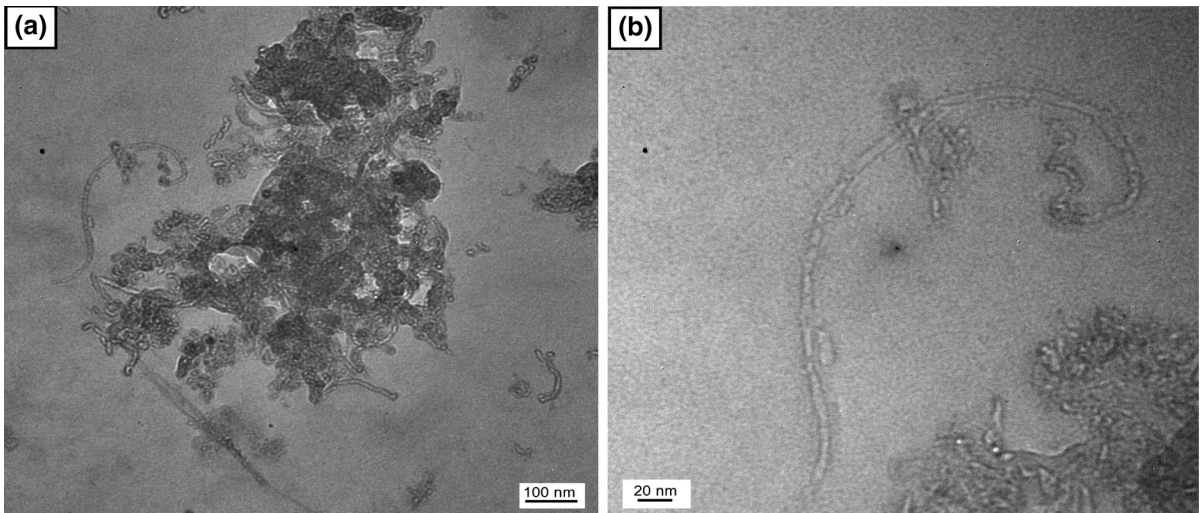


**Fig. 7** The TEM images of BC-g-cMWCNTs **a**  $\times 120,000$ , **b**  $\times 400,000$

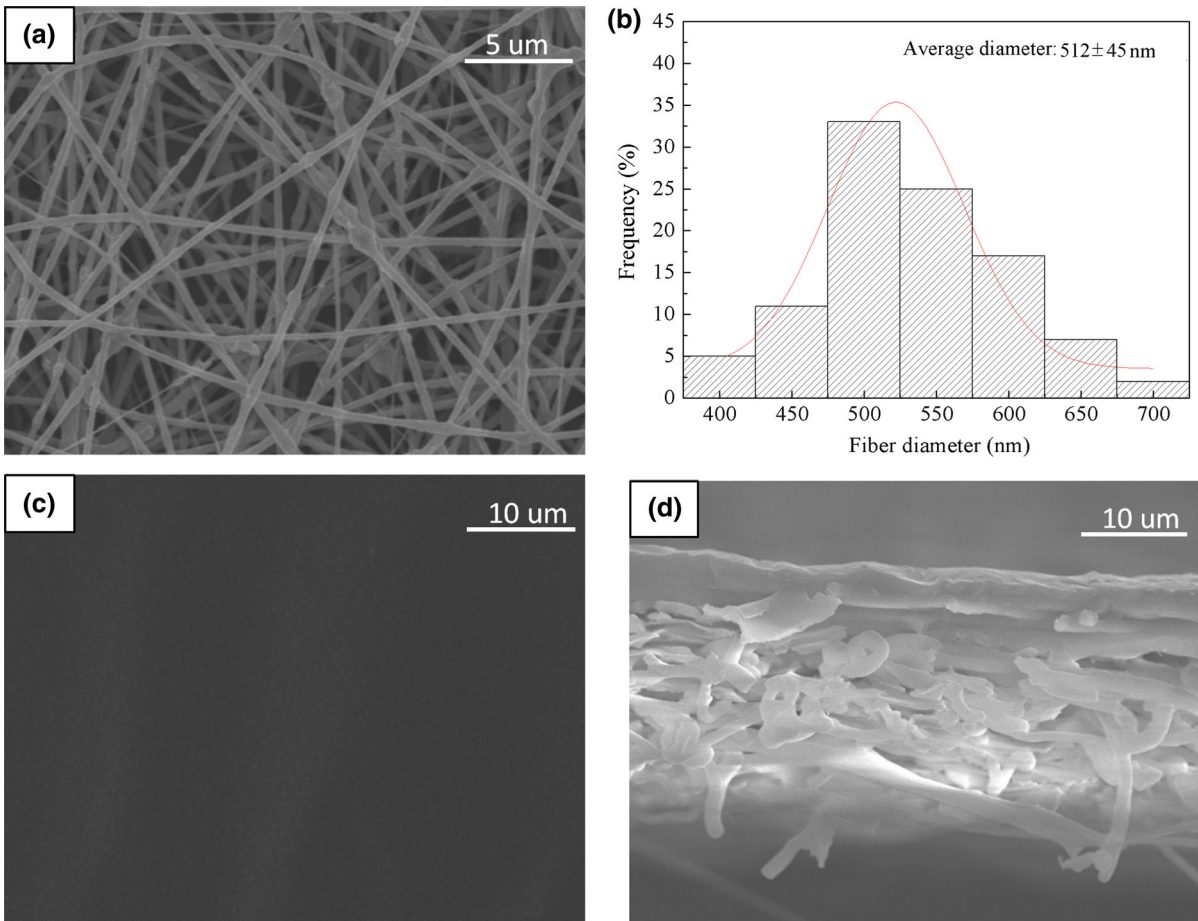


**Fig. 8** The SEM image **(a)** and diameter distribution **(b)** of electrospun BC-g-cMWCNTs nanofiber membrane, the surface **(c)** and cross section **(d)** SEM images of chitosan coated BC-g-cMWCNTs nanofiber composite membrane



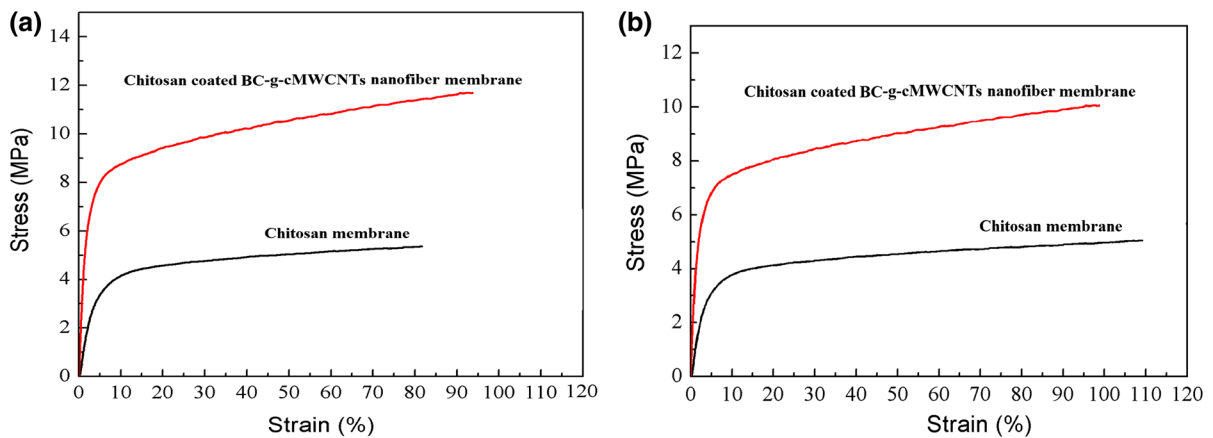


**Fig. 9** The stress–strain curves of chitosan membrane and chitosan coated BC-g-cMWCNTs nanofiber composite membrane. (**a** in dry state, **b** in wet state)

the ductile fracture with elongation at break over 80%. The stress was increased rapidly with the strain increasing to approximately 5% in the linear elastic deformation stages of the initial stretching and then increased slightly in the tensile yield strengthening stage. For chitosan membrane, its tensile strength was about 5.43 MPa in dry state. By introduction of electrospun BC-g-cMWCNTs nanofiber as backbone, the tensile mechanical properties can be greatly improved. As seen from Fig. 9a, the tensile strength of chitosan coated BC-g-cMWCNTs nanofiber composite membrane was increased to 11.76 MPa in dry state, which is more than twice of the chitosan membrane. In order to use chitosan coated BC-g-cMWCNTs nanofiber composite membrane as nanofiltration membrane for dye removal, its mechanical properties in wet state are the key factors. Figure 9b illustrates the wet tensile mechanical properties of chitosan membrane and chitosan coated BC-g-cMWCNTs nanofiber composite membrane. The tensile strength was slightly decreased to 5.06 and 10.11 MPa for chitosan membrane and chitosan coated BC-g-cMWCNTs nanofiber composite membrane, respectively.

Table 1 summarized the mechanical properties of chitosan membrane and chitosan coated BC-g-cMWCNTs nanofiber composite membrane. The tensile strength and Young's Modulus were about more than twice of chitosan membrane, indicating that the incorporation of BC-g-cMWCNTs nanofiber could greatly improve the tensile mechanical properties of chitosan coated BC-g-cMWCNTs nanofiber

composite membrane. The reason might be due to the fact that the cMWCNTs were uniformly grafted on BC molecular chains and played a reinforcing and toughening role in the nanofiber membrane.

Chitosan membrane has lower mechanical properties. These results meant that the membrane has big deformation under low operation pressure, which could change the pore size of the membrane resulting in low rejection rate during the filtration of dye solution. Reinforced by BC-g-cMWCNTs nanofiber, the Young's Modulus can be greatly improved as well as the tensile strength. The values was reached to 211 and 10.11 MPa for the Young's modulus and tensile strength, respectively. As seen from Fig. 9b, few strain can be generated under 0.5 MPa for chitosan coated BC-g-cMWCNTs nanofiber composite membrane, which indicated that the pore structure of membrane can keep stable. Using this chitosan coated BC-g-cMWCNTs nanofiber composite membrane for dye removal, the flux could be improved and the rejection rate would not decreased with the operation pressure increased to 0.5 MPa.

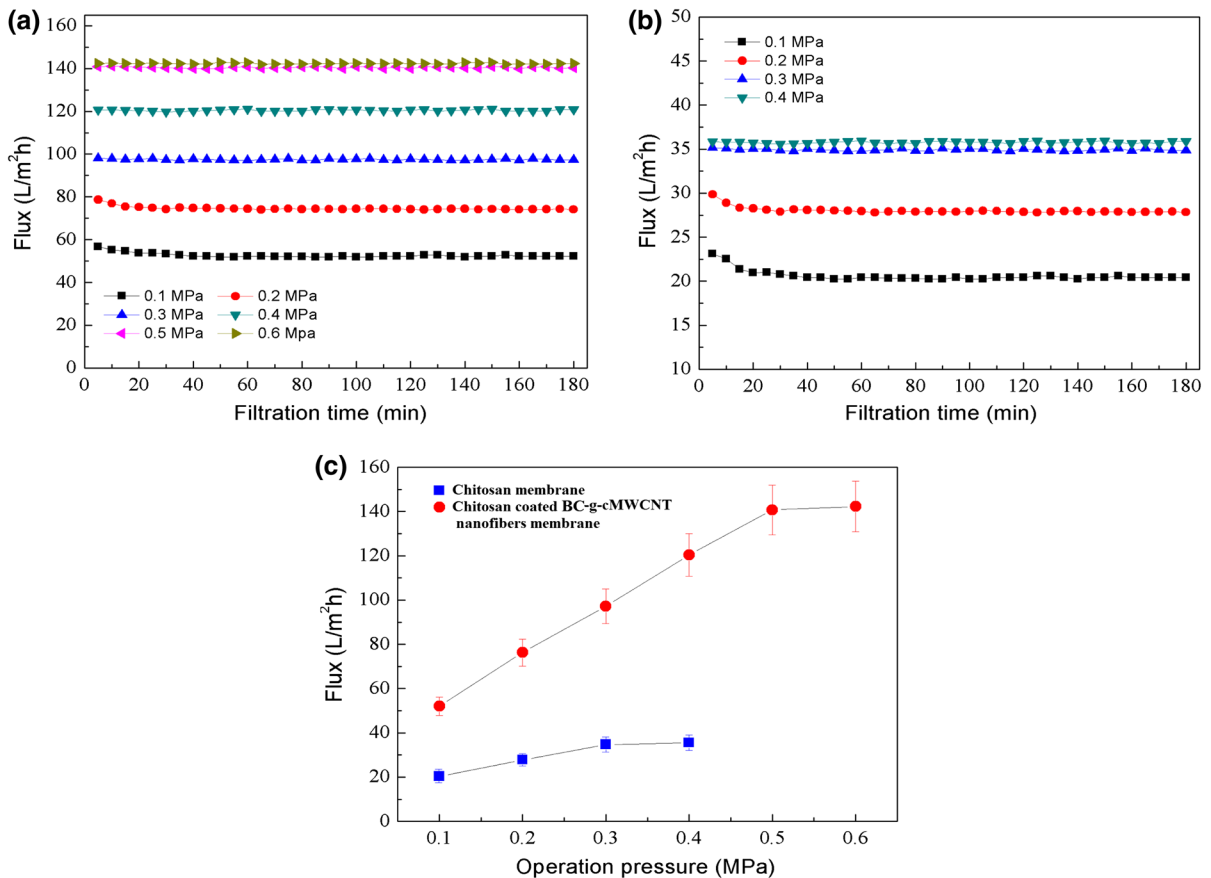
The filtration properties of chitosan coated BC-g-cMWCNTs nanofiber composite membrane

#### *The pure water flux*

Figure 10 shows the effect of filtration time on the pure water flux (PWF) of chitosan coated BC-g-cMWCNTs nanofiber composite membrane under different operation pressure ranged from 0.1 to

**Table 1** Mechanical properties of chitosan membrane and chitosan coated BC-g-cMWCNTs nanofiber composite membrane

	Tensile strength (MPa)	Elongation at break (%)	Young's Modulus (MPa)
Chitosan membrane	5.43 (in dry state) 5.06 (in wet state)	82.6 (in dry state) 109.4 (in wet state)	96.5 (in dry state) 81.4 (in wet state)
Chitosan coated BC-g-cMWCNT nanofiber composite membrane	11.76 (in dry state) 10.11 (in wet state)	94.3 (in dry state) 99.6 (in wet state)	244 (in dry state) 211 (in wet state)

**Fig. 10** The effect of filtration time on the pure water flux (PWF) of chitosan coated BC-g-cMWCNTs nanofiber composite membrane (a) and chitosan membrane (b) under different operation pressure (c)

0.6 MPa using chitosan membrane as comparison. At low operation pressure, the fluxes were slightly reduced at the beginning and kept stable after filtration for 20 min. At high operation pressure, the fluxes were almost kept stable for all filtration process. For chitosan membrane, the PWF was almost increased linearly from 20.3 to 34.7  $L/m^2 h$  with the operation pressure increasing from 0.1 to 0.3 MPa. For chitosan coated BC-g-cMWCNTs nanofiber composite

membrane, the PWF was increased from 52.1 to 140.7  $L/m^2 h$  with the operation pressure increasing from 0.1 to 0.6 MPa. In the range of 0.1–0.5 MPa, this increase was almost linearly. When the operation pressure was above 0.5 MPa, the PWF was tended to become stable with an increase in the operation pressure. The reason might be ascribed to the effective porosity generated by the interconnected pores and the distance of the porous channels, which are the key

points to determine the flux of the filtration membrane. Thus, it would be efficient method to improve flux by increasing the number of interconnected pores or decreasing the thickness of the filtration membrane. When the operation pressure was below 0.3 or 0.5 MPa, the deformation of chitosan membrane and chitosan coated BC-g-cMWCNTs nanofiber composite membrane was very slightly due to its high Young's Modulus (about 81 or 211 MPa). The interconnected pores were maintained adequately and the porous channels were kept stable. With the operation pressure increasing, the PWF was increased linearly. When the operation pressure was increased over 0.3 or 0.5 MPa, the deformation may change the interconnected pores structure and decrease the effective porosity. Whereas, the thickness of the membrane would be also decreased. In the end, the flux was reached an equilibrium value. This chitosan coated BC-g-cMWCNTs nanofiber composite membrane can be operated at 0.5 MPa with PWF of  $140.7 \text{ L/m}^2 \text{ h}$ , which is much higher than that of common filtration membranes ( $114 \text{ L/m}^2 \text{ h}$ ) (Rezzadori et al. 2015).

#### Oil–water emulsion filtration

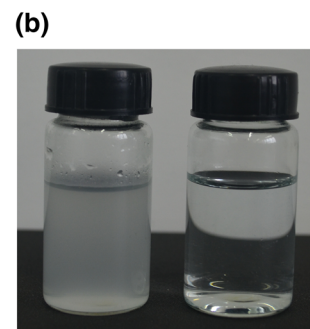
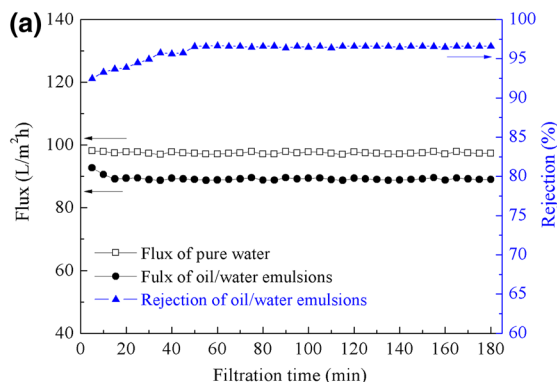
Figure 11a presents the rejection rate and solution flux of chitosan coated BC-g-cMWCNTs nanofiber composite membrane using oil (Tween-80)/water emulsion as feed solution. The flux of oil–water emulsion was slightly reduced at the beginning, but when the filtration time was more than 20 min, the flux was reached stable values at  $88.76 \text{ L/m}^2 \text{ h}$ . The stable flux of oil–water emulsion was 91.46% of the PWF, indicating that chitosan coated BC-g-cMWCNTs nanofiber composite membrane exhibited excellent

anti-fouling property for oil–water emulsion. The rejection rate of oil–water emulsion was about 97.67%. Figure 11b shows the photographs of oil–water emulsion solution before and after filtration. It can be seen the solution becomes clear after filtration due to removal of most of Tween-80 by chitosan coated BC-g-cMWCNTs nanofiber composite membrane.

#### BSA anti-fouling property and Flux recovery rate

Figure 12 illustrates the PWF, flux and rejection rate of BSA solution of chitosan coated BC-g-cMWCNTs nanofiber composite membrane and the alternating filtration flux between pure water and BSA solution under 0.3 MPa operating pressure. The fluxes of BSA solution were slightly decreased at the beginning. After 30 min, the fluxes were reached stable value at  $91.54 \text{ L/m}^2 \text{ h}$ , which is about 94.27% of the PWF. The rejection rate of BSA was about 99.74% and kept stable during the filtration process. At the same time, chitosan coated BC-g-cMWCNTs nanofiber composite membrane showed good water flux recovery property as shown in Fig. 12b. The PWF was decreased slightly from 97.3 to  $96.4 \text{ L/m}^2 \text{ h}$  after feed solution changed from pure water to BSA solution. After three rounds of pure water to BSA solution, the PWF was still reached  $93.4 \text{ L/m}^2 \text{ h}$ , which is about 96% of the initial value without any cleaning operation. The high rejection rate of BSA together with high flux and good flux recovery indicated that chitosan coated BC-g-cMWCNTs nanofiber composite membrane has the advantage of strong protein anti-fouling properties.

**Fig. 11** The flux and rejection rate (a) of oil–water emulsion solution of chitosan coated BC-g-cMWCNTs nanofiber composite membrane under 0.3 MPa and the photographs (b) of emulsion before and after filtration



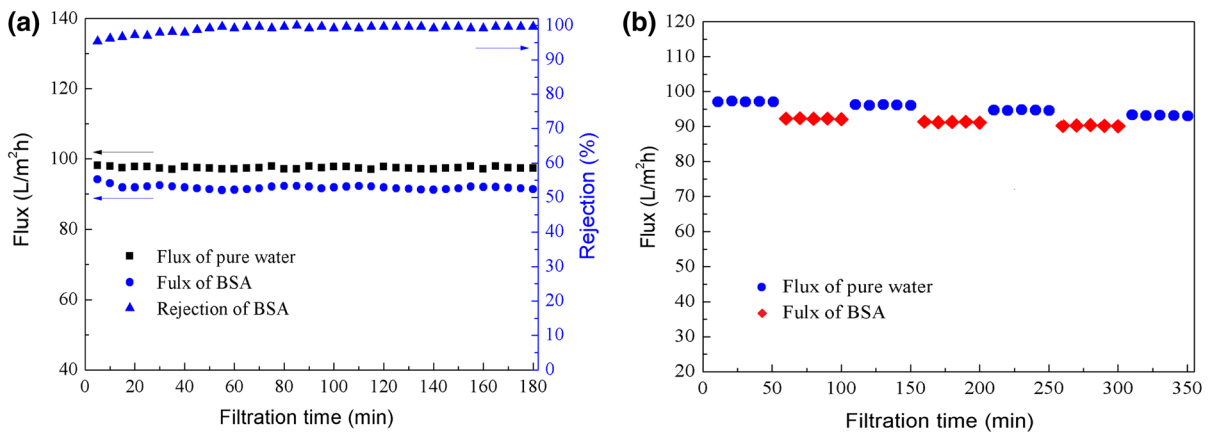


**Fig. 12** The PWF, flux and rejection rate of BSA solution (a), and the alternating filtration flux between pure water and BSA solution (b) of chitosan coated BC-g-cMWCNTs nanofiber composite membrane under 0.3 MPa operating pressure

### Salts rejection

Chitosan coated BC-g-cMWCNTs nanofiber composite membrane presents different rejection to  $\text{MgSO}_4$  and NaCl, as evidenced by the data measured at the same concentration ( $2000 \text{ mg L}^{-1}$ ) at pH 7.0 under 298.15 K in Table 2. The salt rejections followed the order of  $\text{MgSO}_4 > \text{NaCl}$ , which seems to deviate from the prediction based on the Donnan exclusion mechanism. Chitosan coated BC-g-cMWCNTs nanofiber composite membrane is a positively charged membrane due to the protonation of amino groups of chitosan. Thus, the nanofiber composite membrane has a strong ion shielding effect for Magnesium. The  $\text{MgSO}_4$  and NaCl rejection of the new nanofiber composite membrane were about 98.2 and 57%, which were slightly higher than that of commercial NF270.

### Dye solution filtration

Figure 13 gives the flux and rejection rate for dye solution of chitosan coated BC-g-cMWCNTs nanofiber composite membrane under 0.5 MPa operating pressure. Four dyes with different molecular weight ranged from 300 to 800 g/mol were selected for

filtration test. They are Direct Orange S, Procion Red mx-5B, Stilbene Yellow and Methylene Blue with molecular weight 756.67, 615.33, 452.37 and 337.87 g/mol, respectively. For dyes with higher molecular weight such as Direct Orange S and Procion Red mx-5B, the fluxes were slightly decreased with time and finally become stable after about 60 min. For dyes with lower molecular weight such as Stilbene Yellow and Methylene Blue, the fluxes were fluctuated slightly at the beginning and reached stable value quickly. The stable flux and rejection rate for Direct Orange S, Procion Red mx-5B, Stilbene Yellow and Methylene Blue aqueous solution were 132.5, 128.7, 121.2, 115.5  $\text{L/m}^2 \text{ h}$  and 99.7, 97.8, 62.8, 27.5%, respectively.

The operation pressure and molecular weight of dye have important effect on the filtration performances of chitosan coated BC-g-cMWCNTs nanofiber composite membrane as presented in Fig. 14. The fluxes of dye solution were increased with operation pressure increasing, which is consistent with the trend of PWF. For dyes with molecular weight higher than 600 g/mol, such as Direct Orange S and Procion Red mx-5B, the rejection rate still can be 99.1 and 97.5% under 0.5 MPa operation pressure. But for Stilbene

**Table 2** Salts rejection for nano-filtration membranes

Nano-filtration membrane	Rejection (%) in $\text{MgSO}_4$	Rejection (%) in NaCl
NF270	> 97	> 50
Chitosan coated BC-g-cMWCNTs nanofiber composite membrane	$98.2 \pm 1.1$	$57 \pm 1.4$

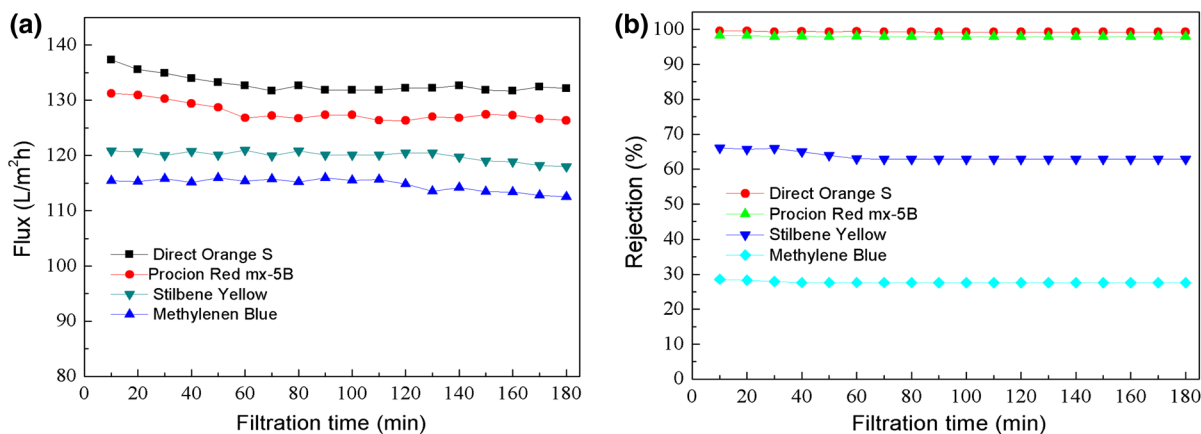


**Fig. 13** The flux (a) and rejection rate (b) for dye solution of chitosan coated BC-g-cMWCNTs nanofiber composite membrane under 0.5 MPa operating pressure

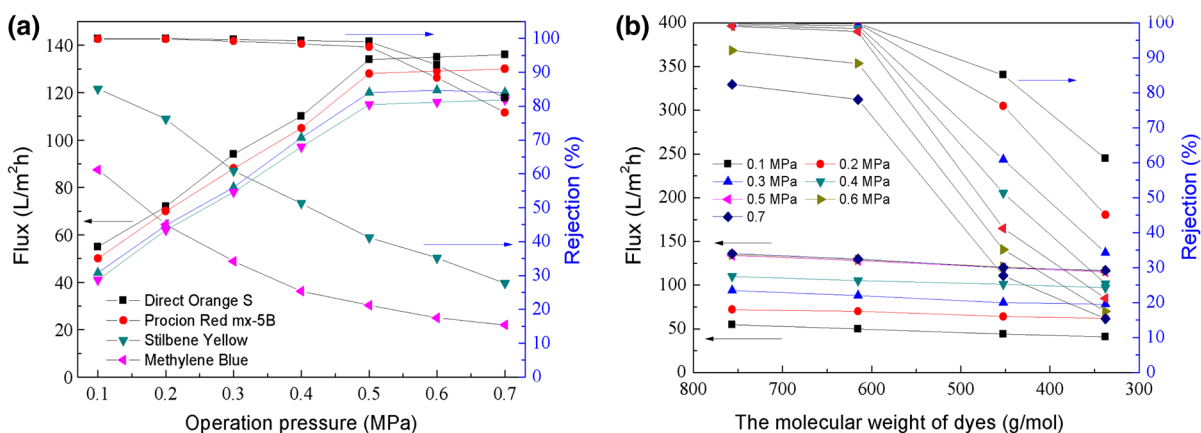


**Fig. 14** The flux and rejection rate of chitosan coated BC-g-cMWCNTs nanofiber composite membrane versus operation pressure (a) and molecular weight of dyes (b)

Yellow and Methylene Blue with molecular weight lower than 600 g/mol, the rejection rate only can be 60.9 and 34.2% under 0.3 MPa, respectively. It seems that this chitosan coated BC-g-cMWCNTs nanofiber composite membrane are more effective for removal of dyes with molecular weight higher than 600 g/mol. It can be operated at 0.5 MPa operation pressure with flux and rejection rate of 125 L/m<sup>2</sup> h and 99.1%. The high flux and rejection rate of chitosan coated BC-g-cMWCNTs nanofiber composite membrane were attributed to higher porosity of electrospun nanofibrous membrane (as supporting layer) and denser thin film of chitosan coating (as barrier layer), respectively. Since the molecular weight of Direct Orange S and Procion Red mx-5B was 756.67 and 615.33 g/mol, that is, the molecular weight cut-off (MWCO) of

membrane was lower than 1000 Da, chitosan coated BC-g-cMWCNTs nanofiber composite membrane belonged to nano-filtration separation technology (Jorio et al. 2003). This chitosan coated BC-g-cMWCNTs nanofiber composite membrane can be used as an efficient nano-filtration membrane with high flux and rejection rate at high pressure for dye removal.

### Conclusions

Chitosan coated BC-g-cMWCNTs nanofiber composite membrane was prepared by combination of electrospinning technology and surface coating method. The electrospun BC-g-cMWCNTs nanofiber as

supporting layer presented excellent tensile mechanical properties and high porosity and the coating layer with denser chitosan thin film was used as barrier layer. This chitosan coated BC-g-cMWCNTs nanofiber composite membrane had the tensile strength and Young's Modulus of 11.75, 10.11 and 244, 211 MPa in dry and wet state, respectively. Filtration test results showed that the PWF was increased from 52.1 to 140.7 L/m<sup>2</sup> h with operation pressure increasing from 0.1 to 0.6 MPa. Direct Orange S, Procion Red mx-5B, Stilbene Yellow and Methylene Blue with molecular weight ranged from 300 to 800 g/mol were selected for dye removal test. The rejection rate of dyes could reach above 90% when the molecular weight of dyes in feed solution was larger than 600 g/mol under 0.5 MPa pressure. Chitosan coated BC-g-cMWCNTs nanofiber composite membrane exhibited good anti-fouling properties for both oil and protein. These results indicated that chitosan coated BC-g-cMWCNTs nanofiber composite membrane can be used as an efficient nano-filtration membrane with high flux and rejection rate at high pressure for dye removal from wastewater.

**Acknowledgments** This work was supported by Tianjin Science Technology Research Funds of China (16JCZDJC37500) and The Project of Tianjin Science and Technology Correspondent (16JCTPJC44800).

## References

- Ahmed FE, Lalia BS, Hashaikeh R (2015) A review on electrospinning for membrane fabrication: challenges and applications. *Desalination* 356:15–30
- Cai Z, Song X, Zhang Q, Liu Y (2017a) Amidoxime surface modification of polyindole nanofiber membrane for effective removal of Cr(VI) from aqueous solution. *J Mater Sci* 52:5417–5434
- Cai Z, Zhang Q, Zhu C, Song X, Liu Y (2017b) Development of a sodium/electrospun poly(5-cyanoindole) nanofiber secondary battery system with high performance. *Synth Met* 231:15–18
- Cai Z, Zhu C, Guo J, Zhang Q, Zhao K (2018) Electrospun carboxyl multi-walled carbon nanotubes grafted polyhydroxybutyrate composite nanofibers membrane scaffolds: preparation, characterization and cytocompatibility. *Mater Sci Eng, C* 82:29–40
- Gasemloo S, Sohrabim M, Khosravim M, Dastmalchim S, Gharbani P (2016) Fabrication of sulfated nanofilter membrane based on carboxymethyl cellulose. *Water Sci Technol* 74:2611–2619
- Guo J, Zhang Q, Cai Z, Zhao KY (2016) Preparation and dye filtration property of electrospun polyhydroxybutyrate–calcium alginate/carbon nanotubes composite nanofibrous filtration membrane. *Sep Purif Technol* 161:69–79
- Huang Y, Huang QL, Liu H, Zhang CX, You YW, Li NN (2017) Preparation, characterization, and applications of electrospun ultrafine fibrous PTFE porous membranes. *J Membrane Sci* 523:317–326
- Jorio A, Pimenta MA, Filho AGS, Saito R, Dresselhaus G, Dresselhaus MS (2003) Characterizing carbon nanotube samples with resonance Raman scattering. *New J Phys* 5:139.1–139.17
- Kaur S, Rana D, Matsuura T, Sundarajan S, Ramakrishna S (2012a) Preparation and characterization of surface modified electrospun membranes for higher filtration flux. *J Membr Sci* 390–391:235–242
- Kaur S, Sundarajan S, Rana D, Matsuura T, Ramakrishna S (2012b) Influence of electrospun fiber size on the separation efficiency of thin film nanofiltration composite membrane. *J Membr Sci* 392–393:101–111
- Kebria MRS, Jahanshahi M, Rahimpour A (2015) SiO<sub>2</sub> modified polyethyleneimine-based nanofiltration membranes for dye removal from aqueous and organic solutions. *Desalination* 367:255–264
- Khorshidi S, Solouk A, Mirzadeh H, Mazinani S, Lagaron JM, Sharifi S (2016) A review of key challenges of electrospun scaffolds for tissue-engineering applications. *J Tissue Eng Regen Med* 10:715–738
- Lalia BS, Kochkodan V, Hashaikeh R, Hilal N (2013) A review on membrane fabrication: structure, properties and performance relationship. *Desalination* 326:77–95
- Li XP, Chen YB, Hu XY, Zhang YF, Hu LJ (2014) Desalination of dye solution utilizing PVA/PVDF hollow fiber composite membrane modified with TiO<sub>2</sub> nanoparticles. *J Membr Sci* 471:118–129
- Liang CZ, Sun SP, Li FY, Ong YK, Chung TS (2014) Treatment of highly concentrated wastewater containing multiple synthetic dyes by a combined process of coagulation/flocculation and nanofiltration. *J Membr Sci* 469:306–315
- Liu W, Zhu L, Huang C, Jin X (2016) Direct electrospinning of ultrafine fibers with interconnected macropores enabled by in situ mixing microfluidics. *Appl Mater Interf* 8:34870–34878
- Makaremi M, Lim CX, Pasbakhsh P, Sui ML, Goh KL, Chang H (2016) Electrospun functionalized polyacrylonitrile-chitosan bi-layer membranes for water filtration applications. *RSC Adv* 6:53882–53893
- Rajesh S, Senthilkumar S, Jayalakshmi A, Nirmala MT, Ismail AF, Mohan D (2013) Preparation and performance evaluation of poly (amide-imide) and TiO<sub>2</sub> nanoparticles impregnated polysulfone nanofiltration membranes in the removal of humic substances. *Colloid Surface A* 418:92–104
- Rezzadori K, Penha FM, Proner MC, Zin G, Petrus JCC, Prádanos P, Palacio L, Hernández A, Luccio MD (2015) Evaluation of reverse osmosis and nanofiltration membranes performance in the permeation of organic solvents. *J Membr Sci* 492:478–489
- Rosa RM, Silva JC, Sanches IS, Henriques C (2017) Simultaneous photo-induced cross-linking and silver nanoparticle formation in a PVP electrospun wound dressing. *Mater Lett* 207:145–148

- Urban J (2016) Current trends in the development of porous polymer monoliths for the separation of small molecules. *J Sep Sci* 39:51–68
- Wang XF, Zhang K, Yang Y, Wang LL, Zhou Z, Zhu MF, Hsiao BS, Chu B (2010) Development of hydrophilic barrier layer on nanofibrous substrate as composite membrane via a facile route. *J Membr Sci* 356:110–116
- Wenhui S, Zhen Z, Weiliang T, Xinling W (2007) A facile approach to covalently functionalized carbon nanotubes with biocompatible polymer. *Polymer* 48:3658–3663
- Wu D, Huang Y, Yu S, Lawless D, Feng X (2014) Thin film composite nanofiltration membranes assembled layer-by-layer via interfacial polymerization from polyethylenimine and trimesoyl chloride. *J Membr Sci* 472:141–153
- Xu L, Du LS, Wang C, Xu W (2012) Nanofiltration coupled with electrolytic oxidation in treating simulated dye wastewater. *J Membr Sci* 409–410:329–334
- Yang S, Shao D, Wang X, Hou G, Nagatsu M, Tan X (2015) Design of chitosan-grafted carbon nanotubes: evaluation of how the –OH functional group affects Cs<sup>+</sup> adsorption. *Mar Drugs* 13:3116–3131
- Yoon K, Hsiao BS, Chu B (2009) High flux nanofiltration membranes based on interfacially polymerized polyamide barrier layer on polyacrylonitrile nanofibrous scaffolds. *J Membr Sci* 326:484–492
- Yoon JT, Lee SC, Jeong YG (2010) Effects of grafted chain length on mechanical and electrical properties of nanocomposites containing polylactide-grafted carbon nanotubes. *Compos Sci Technol* 70:776–782
- Zeng G, He Y, Zhan Y, Zhang L, Pan Y, Zhang C, Yu Z (2016) Novel polyvinylidene fluoride nanofiltration membrane blended with functionalized halloysite nanotubes for dye and heavy metal ions removal. *J Hazard Mater* 317:60–72
- Zhang XX, Lin BB, Zhao KY, Wei JF, Guo J, Cui WK, Jiang S, Liu D, Li JX (2015) A free-standing calcium alginate/polyacrylamide hydrogel nanofiltration membrane with high anti-fouling performance: preparation and characterization. *Desalination* 365:234–241
- Zhang M, Zhao X, Zhang G, Wei G, Su Z (2017) Electrospinning design of functional nanostructures for biosensor applications. *J Mater Chem B* 5:1699–1711
- Zhao S, Wang Z (2017) A loose nano-filtration membrane prepared by coating HPAN UF membrane with modified PEI for dye reuse and desalination. *J Membr Sci* 524:214–224
- Zheng YP, Yao GH, Cheng QB, Yu SC, Liu MH, Gao CJ (2013) Positively charged thin-film composite hollow fiber nanofiltration membrane for the removal of cationic dyes through submerged filtration. *Desalination* 328:42–50
- Zhou CM, Shi YL, Sun CS, Yu SC, Liu MH, Gao CJ (2014) Thin-film composite membranes formed by interfacial polymerization with natural material sericin and trimesoyl chloride for nanofiltration. *J Membr Sci* 471:381–391
- Zhu H, Szymczyk A, Balanec B (2011) On the salt rejection properties of nanofiltration polyamide membranes formed by interfacial polymerization. *J Membr Sci* 379:215–223
- Zhu WP, Gao J, Sun SP, Zhang S, Chung TS (2015) Poly(amidoamine) dendrimer (PAMAM) grafted on thin film composite (TFC) nanofiltration (NF) hollow fiber membranes for heavy metal removal. *J Membr Sci* 487:117–126
- Zhu M, Han J, Wang F, Shao W, Xiong R, Zhang Q (2017) Electrospun nanofibers membranes for effective air filtration. *Macromol Mater Eng* 302:1600353